Dynamic Behavior of Liquid Propellant in Reusable Rocket Vehicle

HIMENO Takehiro
Department of Aeronautics and Astronautics, University of Tokyo,
7-3-1, Hongo, Bunkyo-ku, Tokyo, 113-8656 JAPAN.
himeno@aero.t.u-tokyo.ac.jp
and
NONAKA Satoshi, NARUO Yoshihiro and INATANI Yoshifumi
Institute of Space and Astronautical Sciences, Japan Aerospace Exploration Agency.
and
WATANABE Toshinori
Department of Aeronautics and Astronautics, University of Tokyo

Keywords : Propellant Management, Liquid Propulsion, Sloshing, RLV, CFD

Abstract

For the prediction of sloshing in the propellant tank of rocket vehicle utilized in RVT (reusable rocket vehicle testing) conducted by ISAS/JAXA, the flow field in the propellant tank during the ballistic flight was experimentally reproduced with the sub-scale model of it. The lateral acceleration as large as about 0.8 G was provided with a mechanical exciter and the deformation of liquid surface in the vessel was visualized with a high-speed camera. The several configurations of damping devices were installed and tested in the vessel, which should keep the ullage gas away from the outlet port. It was consequently suggested that the combination of a baffle plate and a perforated cylinder could be effective against the gas suction before the re-ignition of the engine. The sloshing phenomena were also simulated with the CFD code, called CIP-LSM. The numerical results showed good agreement with the corresponding data obtained in the experiment.

Introduction

Figure 1 shows the flight of a rocket vehicle conducted by ISAS/JAXA, the Institute of Space and Astronautical Sciences. In the series of the reusable rocket vehicle testing, RVT [1], demonstrated the vertical landing, repeated flight capabilities and turnaround characteristics. The liquid hydrogen-propelled vehicle, shown in Fig.2, was designed to provide the opportunities for the studies and investigations on the technical issues as to the realization of reusable launch vehicle (RLV) in the future, such as flight on demand, quick turnaround, higher performance, light weight structures and materials and so on. The performance of the test vehicle at present is still limited, however, many lessons were learned and more flight will be conducted to improve the performance of hardware and software through the flight operations.

Propulsion System

The propulsion system of the test vehicle acquires the capability of re-ignition, which enables the rocket engine to burn more than two times during the flight. It is not only a minimum function for the vertical landing after the ballistic flight, but also the potential for the various sequences such as sounding missions or aborting operations in the future.

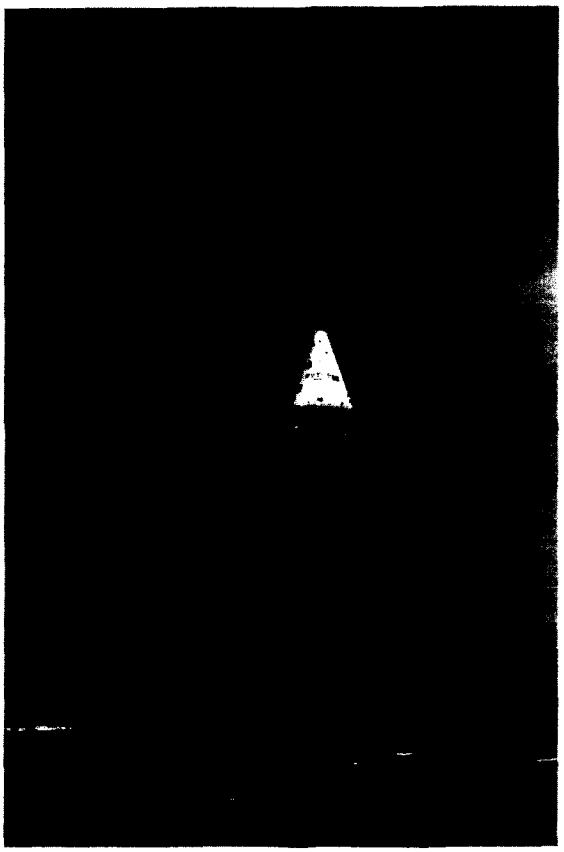

Fig.1 : Reusable Rocket Vehicle Testing (RVT), conducted by ISAS / JAXA at Noshiro Testing Center in 2003.

Gravity Environment

Nevertheless, from a view of the propellant management [2-3], it becomes very difficult to keep the liquid propellant in desirable position in the tank

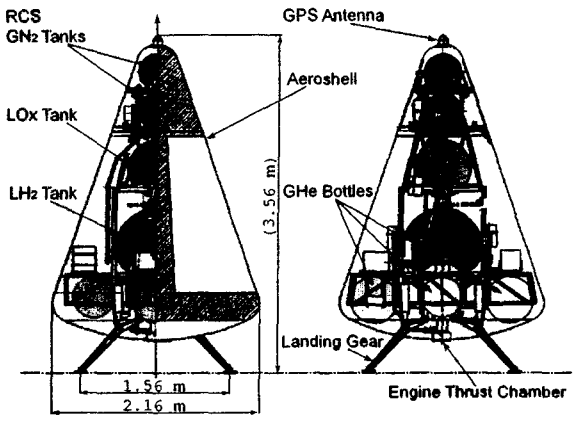

Fig.2 : Perspective drawing of the test vehicle, utilizing LOX and LH_2 as propellants for the pressure-fed-type engine.

under the low-gravity condition during the ballistic flight. From the viewpoint, the possibility of the ballistic flight at low altitude is considered for the future campaign of RVT.

Figure 3 shows the acceleration of the test vehicle as a function of time estimated by the flight simulator. In this case, the main engine will be cut off once at about 8.0 sec after the lift-off, ignited again at about 12.0 sec and the decelerated vehicle will land vertically at about 19.0 sec. In the period of ballistic flight for about 4.0 sec, as is shown in the right chart, the vertical acceleration by aerodynamic force is possible to be as small as 0.01 G. Since it could be the similar level to the lateral acceleration induced by the side wind with a speed of 5 meters a second, there is concern that the sloshing of liquid propellant with large amplitude should take place in the tank. If the large amount of gaseous helium, which is utilized for pressurization, should be sucked through the outlet port located on the bottom of the tank and reach at the combustion chamber, it might result in the failure of re-ignition sequence and, in the worst case scenario, the loss of the vehicle.

Experimental Assessment

In order to give appropriate assessment on the dynamic behavior of liquid propellant during the ballistic flight, the sloshing motion in the small vessel was experimentally investigated. The second purpose of the experiment was to obtain the visualized data for the check of correlation with the numerical results.

Experimental Facilities

Figure 4 shows the mechanical exciter manufactured for the present experiment, which was composed of a stepping motor, a rack-and-pinion transmission and a slider. The model tank made of poly-acrylic resin was mounted on the slider and could be accelerated in the lateral direction up to about 1.0 G. As is shown in Fig.5, the model tank, 0.20m in diameter, was consist of a cylindrical part, an upper and a lower dome, which was similar to the LH_2 tank of the test vehicle with about 1/3.2 contraction dimension. There was a round bar along the center axis, which corresponded to the feed line in the real tank. In addition, as the devices for the damping of liquid motion, a conic-shaped baffle with round holes and a perforated cylinder could be equipped inside of the tank.

Similar Flow

In the present study, the main concern was focused on whether the anti-slosh devices have effect on preventing the vapor from getting at the outlet port still in the environment where the vertical and lateral acceleration come to be comparable. As operating fluid, utilized water H_2O at ambient temperatures and normal pressures. The unsteady deformation of liquid surface was observed with a high-speed camera through the transparent wall of the vessel.

Figure 6 shows the displacement of the slider as a function of time, which was programmed and controlled by PC. In the experiments described in this section, the lateral acceleration provided by the mechanical exciter was varied linearly from −0.8G to 0.8G in 0.48 sec, while the vertical acceleration was

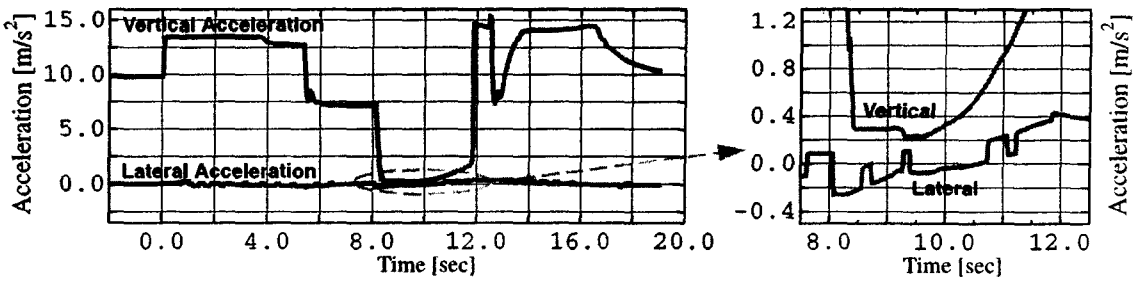

Fig.3 : Time Variation of Acceleration on the Vehicle; Estimated by the Flight Simulator; Main Engine Cut off at about 8.0 sec and Re-ignition at about 12.0 sec; The Lateral Acceleration is Comparable to the Vertical Acceleration.

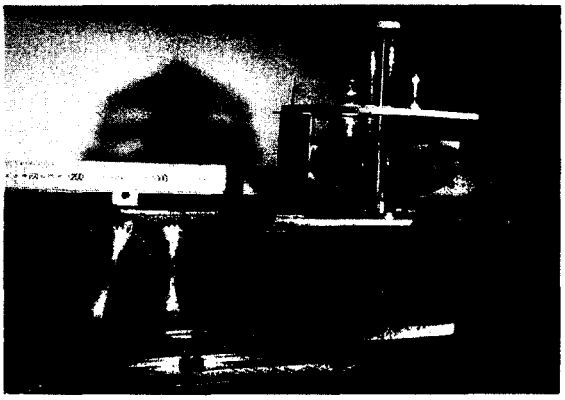

Fig.4 : The model tank mounted on the mechanical exciter.

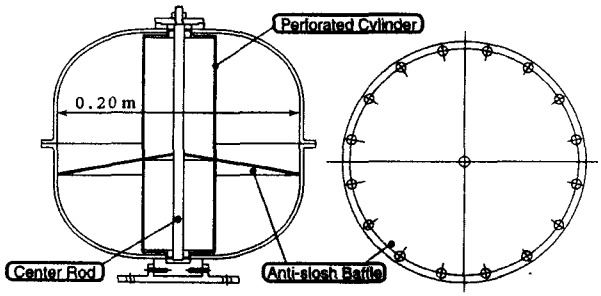

Fig.5 : The configuration of model tank and anti-slosh devices; D = 0.20m.

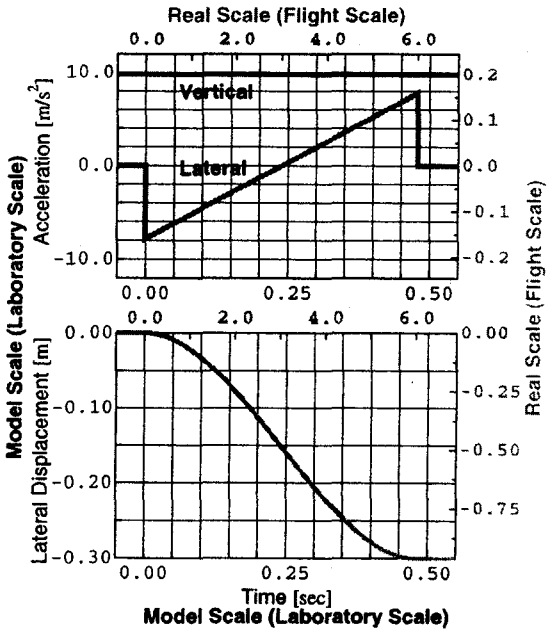

Fig.6 : Displacement of slider provided by a mechanical exciter in Case 1 and Case 2; lateral acceleration is 0.8G at maximum;

fixed as 1.0G, that is, the gravity acceleration on the ground.

If one agree on the similarity rule in terms of Froude number between the free-surface flows in the model tank and those in the real one, it is possible that the liquid motion observed in the laboratory scale be transformed similarly into that in the flight scale.

Experimental Results

Figure 7 shows the visualized flow field in the model tank. In this case, Case 1, the initial level of liquid surface was set to be 0.08m from the bottom and the anti-slosh devices in the vessel, the baffle and cylinder, were removed. Since there is no blockage except for the center rod against the liquid motion, the liquid was once swayed by the inertial force to the right and swung back to the left. It was observed that the inclination of liquid surface got larger than the angular amplitude of acceleration vector, the liquid wave reached the top of the tank and finally broke down. At the same time, the large amount of gas phase was caught in the liquid wave, broke up into small bubbles and floated near the outlet port.

In Case 2, both of the baffle plate and perforated cylinder were installed to resist the sloshing, while the

(a) 0.24 [sec] (b) 0.48 [sec]

Fig.7 : Sloshing in the model tank in Case 1; Without anti-slosh devices; Visualized with a high-speed camera; Water as operating fluid; Acceleration lateral : vertical = 0.8 : 1.0;

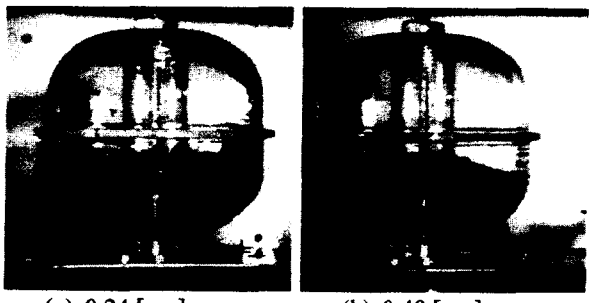

(a) 0.24 [sec] (b) 0.48 [sec]

Fig.8 : Sloshing in the model tank in Case 2; With anti-slosh devices; Visualized with a high-speed camera; Water as operating fluid; Acceleration lateral : vertical = 0.8 : 1.0;

other conditions were not changed from Case 1. In this case, as is shown in Fig.8, the surface deformation was observed to be considerably smaller than that in Case 1. Indeed, a small amount of vapor was still entrained and broken up, however, most of the bubbles were found to be kept away from the bottom of the vessel. Hence, it was consequently suggested that the anti-slosh devices of these should be fairly effective against the gas suction before re-ignition.

Limit of ground tests

Though the catastrophic gas suction was expected to be prevented with the anti-slosh devices, the numerical investigation based on computational fluid dynamics, CFD, was still desired for the more precise assessment, because it was practically impossible on the ground to reproduce the unsteady acceleration in the vertical direction and it was also difficult to carry out the experiments with the flight-scale tank containing cryogenic propellants.

Numerical Approach

To establish the fundamental technology on the basis of CFD for propellant management in space transportation systems, a numerical method to simulate three dimensional free-surface flows under various gravity conditions, called CIP-LSM [4-5], is under development in University of Tokyo and JAXA.

In the present report, the flow fields observed in the experiments were numerically simulated with CIP-LSM, and the computed results were compared with the experimental data for validation.

Basic Equations

In this method, CCUP [6], CIP Combined Unified Procedure, is coupled with LSM [7], Level Set Method and MARS [8], Multi-interface Advection and Reconstruction Solver. No-slip of velocity between gas phase and liquid phase is assumed. Both gas and liquid flows are described by Navier-Stokes equations for homogeneous two-phase flow as follows;

$$\frac{\partial \rho}{\partial t} + (\vec{u} \cdot \nabla)\rho = -\rho \nabla \cdot \vec{u}, \quad (1)$$

$$\rho \frac{\partial \vec{u}}{\partial t} + \rho(\vec{u} \cdot \nabla)\vec{u} = \nabla : \Pi + \vec{g}, \quad (2)$$

$$\rho \frac{\partial e}{\partial t} + \rho(\vec{u} \cdot \nabla)e = \{\Pi : \nabla\} \cdot \vec{u} - \nabla \cdot \vec{q}, \quad (3)$$

where ρ, $\vec{u}$ and e denote density, velocity and energy respectively, and the vectors $\vec{g}$ and $\vec{q}$ appear in the right-hand-sides mean gravity and heat flux. The stress tensor Π includes the tensors of pressure $p\mathbf{I}$, surface tension $\mathbf{T}_\sigma$ and viscous force $\mathbf{T}_\nu$. With unit vector perpendicular to gas-liquid interface denoted by $\vec{n}_S$, each tensor is written as follows;

$$\Pi = -p\mathbf{I} + \mathbf{T}_\sigma + \mathbf{T}_\nu, \quad (4)$$

$$\mathbf{T}_\sigma = \sigma(\mathbf{I} - \vec{n}_S \vec{n}_S)(dH_\varepsilon / d\phi), \quad (5)$$

$$\mathbf{T}_\nu = \lambda(\nabla \cdot \vec{u})\mathbf{I} + \mu(\nabla \vec{u} + \nabla \vec{u}^T), \quad (6)$$

where σ, λ and μ represent the coefficients of surface tension, first and second viscosity, respectively.

To specify the fluid phase at a certain point in the computed domain, the level set function ϕ is introduced, which has as much value as the signed distance from gas-liquid interface. In addition, the extended Heaviside function H_ε is defined as Eq.(7) and the physical properties, such as ρ or μ, were expressed by Eq.(8) at an arbitrary stencil.

$$H_\varepsilon = 0.5 \cdot \max\left[-1.0, \min\left\{1.0, \frac{\phi}{\varepsilon} + \frac{1}{\pi}\sin\left(\frac{\pi\phi}{\varepsilon}\right)\right\}\right]. \quad (7)$$

$$\rho = 0.5\,(\rho_{Liq} + \rho_{Gas}) + H_\varepsilon(\rho_{Liq} - \rho_{Gas}). \quad (8)$$

Conditions

Figure 9 shows the configuration of the computed domain which was similar to the model tank. In the computation, the center rod and the anti-slosh baffle were considered, though the round holes on the baffle plate were changed to the rectangular ones of the equivalent area. In addition, the existence of the perforated cylinder was replaced with drag force and added to the right-hand-side of Eq.(2), resistance coefficient of which was 1.5×10^2.

In this computation, the operating fluids were liquid water and gaseous helium (GHe). The liquid phase was supposed to be incompressible and the gas phase should obey ideal gas equation. At initial, the level of liquid surface was as high as 0.08m from the bottom and the temperature of each phase was given as 298.15 K, while the pressure was set to be about 1.0×10^5 Pa. The flow field was assumed to be plane symmetric and solved only the half around of the tank with 50 x 90 stencils in a meridian section and 36 stencils in the circumferential direction.

As the boundary condition on the surfaces of the tank liner, the center rod and the anti-slosh baffle, both the non-slip and the wetting conditions were

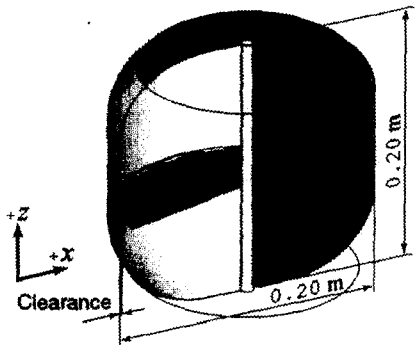

Fig.9 : Computed Domain and Grid System for the Model Tank with 50 x 90 x 36 Stencils.

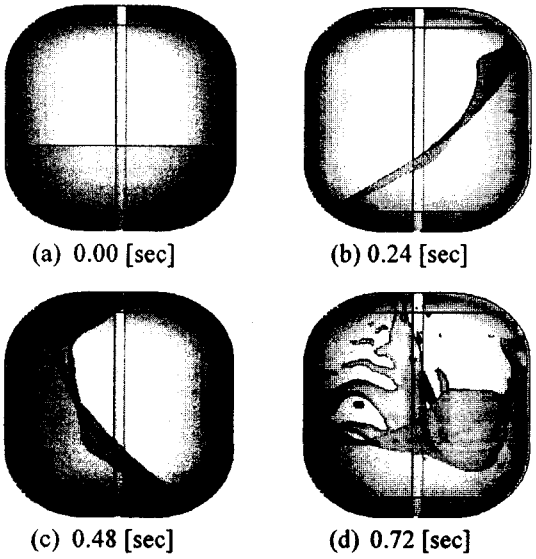

(a) 0.00 [sec] (b) 0.24 [sec]

(c) 0.48 [sec] (d) 0.72 [sec]

Fig.10 : Sloshing in the model tank without anti-slosh devices; Case 3; Computed results corresponded to Case 1.

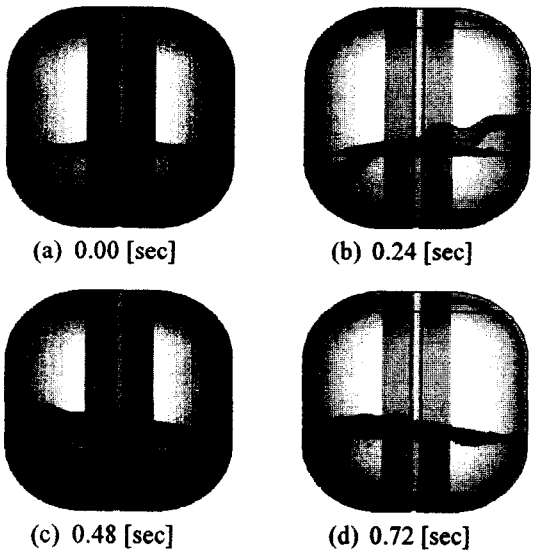

(a) 0.00 [sec] (b) 0.24 [sec]

(c) 0.48 [sec] (d) 0.72 [sec]

Fig.11 : Sloshing in the Model Tank with Anti-slosh Devices; Case 4; Computed Results Corresponded to Case 2.

imposed. The vertical and lateral acceleration were varied as Fig.6.

Results without Anti-slosh Devices

At first, in Case 3, the flow field of Case 1 was numerically simulated. In this case, the anti-slosh devices were removed.

Figure 10 shows the time variation of the computed flow field, the liquid phase was visualized by painted region where the value of ϕ was positive. Compared with the experimental results shown in Fig.7, the cap of the wave at 0.24 sec, the liquid reaching the top at 0.48sec and the following break-down were clearly reproduced in the computation. It is therefore possible to say that CIP-LSM could capture the three-dimensional deformation of liquid surface driven by inertial force and the numerical solution should be fairly accurate.

Results with Anti-slosh Devices

In the next case, Case 4, the flow field of the Case 2 was simulated with the anti-slosh devices equipped in the domain.

Figure 11 shows the computed results visualized in the same way as in Case 3. It was seen that the swaying of the liquid was considerably suppressed, as was observed in the experiment, and the motion of the surface near the anti-slosh baffle was similar to that in Case 2. Even though the bubbles and droplets smaller than the grid scale could not be captured because of the limited resolution, it is possible to say that liquid motion could be simulated with the developed code, and that the thin obstacle, like the anti-slosh baffle, could be included in the computed domain.

Consequently, as far as the main concern was focused on the surface deformation, good agreements were obtained between the numerical results and the experimental data.

Further Investigation

As the next step, the flow fields in the real-scale tank are being simulated under the practical condition of acceleration. It is expected to obtain more appropriate assessment on the dynamic behavior of liquid propellant during the ballistic flight.

Conclusion

In this report, the sloshing problem in the propellant tank of a reusable rocket vehicle during its ballistic flight was both experimentally and numerically investigated.

In the experiment, the dynamic motions of liquid surface in the model-scale tank driven by the mechanical exciter were successfully visualized. The observed flow-field could be translated into the real-scale tank in accordance with the similarity rule in terms of Froude number. It was found that the anti-slosh baffle equipped in the tank could effective to resist the swaying motion of the liquid and be expected to prevent the catastrophic gas-suction even in severe environment where the vertical acceleration became comparable to the lateral one.

Then, the flow fields observed in the experiment were numerically simulated with CIP-LSM. Though the bubbles and droplets smaller than the grid scale were not captured, as far as the main concern was focused on the surface deformation, fairly good agreement was obtained between the numerical results and the experimental data.

As is demonstrated in the present paper, the numerical analysis has a potential to provide helpful assessments for propellant management in a cost-effective manner. Indeed, the computational method of CIP-LSM is now under development. The further improvements and investigations are expected to clarify the various aspects of free-surface flows for the establishment of fluid-management technologies in the space transportation systems [9].

References

1) Y. Inatani, Y. Naruo and K. Yonemoto, *J. Spacecraft and Rockets, AIAA*, vol.38 (2001), No.1, pp.36-42
2) W. C. Reynolds and H. M. Statterlee (1966), *NASA SP-106*, pp.387-449.
3) Basil. N. Antar and Vappu S. Nuotio-Antar (1993), *Fundamentals of Low Gravity Fluid Dynamics and Heat Transfer*, CRC Press, ISBN 0-8493-8913-5.
4) T. Himeno, T. Watanabe and A. Konno (2001), *AIAA 2001-3822.*
5) T. Himeno and T. Watanabe, *Trans. JSME Ser.B*, vol.69 (2003), No.687, pp.2400-2407(in Japanese)
6) T. Yabe, *J. Comput. Phys.*, vol.169 (2001), pp.556-593
7) M. Sussman, P. Smereka, and S. Osher, *J. Comput. Phys.*, vol.114 (1994), pp.146-159
8) T. Kunugi, S. Satake and Y. Ose, *Int. J.Heat and Fluid Flow*, vol.22 (2001), pp.245-251
9) *http://park.itc.u-tokyo.ac.jp/jetlab/*

Acknowledgements

In the planning stage for the present experiment, a lot of advices were provided by Prof. Kaneko in University of Tokyo. The flight simulation shown in Fig.3 was provided by Mr. Maruyama in KHI, Kawasaki Heavy Industries. The authors give their great thanks to them.